

Supporting Information

Polyoxometalate@MOF derived porous carbon-supported MoO₂/MoS₂ octahedron boosting high-rate lithium storage

*Jian Yu,^a Ming-Liang Wang,^a Zhong-Xi Yang,^a Kui Li,^a Xiao-Peng Yang,^a Guang-
Gang Gao,^{*a} Di Yin,^a Lin-Lin Fan,^{*a} Hong Liu^a*

School of Materials Science and Engineering, Collaborative Innovation Center of
Metal Nanoclusters & Photo/Electro-Catalysis and Sensing, University of Jinan,
250022, Jinan, China

Corresponding Authors: mse_gaogg@ujn.edu.cn; mse_fanll@ujn.edu.cn

Contents

Materials: l-glutamic acid, cupric acetate monohydrate, molybdophosphoric acid, 1,3,5-benzenetricarboxylic acid, sulfur powders. Solvents and raw materials were purchased as analytical grade. All chemical reagents were directly used without any purification.

Materials characterization: The morphologies of samples were analyzed by SEM (FEG-250, 30 kV) and TEM (JEM-2100F, 200 kV) equipped with an energy dispersive spectroscope. The structures of the samples were identified by XRD (Rigaku Ultima IV) with Cu K α radiation (50 kV). X-ray photoelectron spectroscopy (XPS) were obtained via the VG ESCALAB MK II X-ray photoelectron spectrometer (the C1s of carbon was calibrated as around 284.6 eV). FTIR spectra were obtained using a NEXUS-870 spectrophotometer with KBr pellets. Thermogravimetric analysis (TGA) of samples were performed on Pyris Diamond6000 TG/DTA thermogravimetric analyzer in air condition. The specific surface area of as-obtained sample was determined by the Brunauer-Emmett-Teller (BET) nitrogen adsorption/desorption method (Quadratorb SI-MP, Quantachrome).

Electrochemical measurements: Active materials (70 wt%), polyvinylidene fluoride (20 wt%) and conductive carbon black (10 wt%) were mixed in N-methyl pyrrolidone (NMP) solvent to form a slurry. The slurry was coated on copper foil and then dried in a vacuum drying oven. The active electrode loading was about 0.8~1.0 mg cm⁻². The half-cell (2032 coin cell) was fabricated with the counter electrode of lithium

metal plate, the electrolyte of 1.0 M LiPF₆ (in 1:1 volume ratio of ethylene carbonate and dimethyl carbonate solvent) and the separator of porous polypropylene in the glove box (oxygen and moisture contents less than 0.1 ppm). All cells were tested using the common LANHE CT2001A battery tester between fixed voltage limits of 0.01 to 3.0 V. CV measurements were performed between 0.01 and 3.0 V via a CHI 660E electrochemistry workstation (ChenHua, China), which was also used to record EIS of cells with a potential amplitude of 5 mV and frequency ranging from 100 kHz to 0.01 Hz.

The operation detail for the mass of the active materials: 10 pieces of copper foils were weighed, and the average weight of copper foils was calculated to be 6.84 mg. Then the active material mass was calculated using a conventional algorithm, namely, the electrode weight subtracted the average weight of copper foils, and then the 70% of the calculated result was the active material mass of electrode. Furthermore, the capacity was calculated according to the mass of the composite to analyze the electrochemical performance.

Supporting figures

Fig. S1 FTIR spectra of PMo₁₂, HKUST-1, and NENU-5.

Fig. S2 XRD pattern of (a) NENU-5 and (b) HKUST-1.

Fig. S3 SEM images of (a) C-MoO₂ and (b) C-MoO₂/MoS₂.

Fig. S4 (a) N₂ adsorption-desorption isotherm of C-MoO₂/MoS₂, (b) pore size distribution curve of C-MoO₂/MoS₂.

Fig. S5 The survey XPS spectra of C-MoO₂ and C-MoO₂/MoS₂.

Fig. S6 (a) The capacity retention of C-MoO₂ and C-MoO₂/MoS₂ at 100, 200, 500, 1000, and 2000 mA g⁻¹, (b) rate capability of C-MoO₂/MoS₂ at 0.2, 0.5, 1, 2, 5, and 10 A g⁻¹.

Fig. S7 Capacitive contribution (shaded region) of C-MoO₂/MoS₂ at the scan rate of 0.8 mV s⁻¹.

Fig. S8 CV curves of (a) C-MoO₂ and (b) C-MoO₂/MoS₂ in the potential range of 0.01~3.0 V with different scan rates (0.2, 0.4, 0.6, 0.8 and 1.0 mV s⁻¹). CV data is collected once the cell is post run for the first cycle to allow the formation of the SEI layer.

Fig. S9 The R_{ct} values of the C-MoO₂ and C-MoO₂/MoS₂.

Table S1 Rate performance of C-MoO₂/MoS₂ compared with other previously reported MoO₂/MoS₂-based anodes in the literatures.

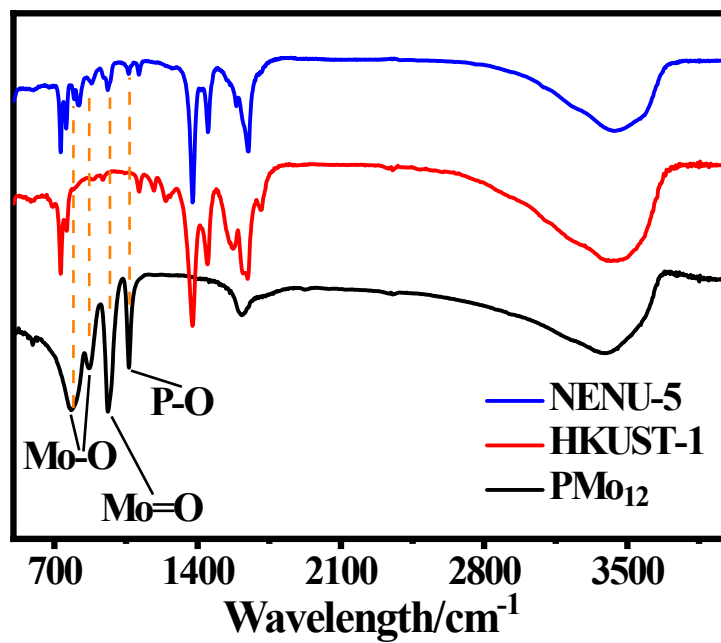


Fig. S1 FTIR spectra of PMo₁₂, HKUST-1, and NENU-5.

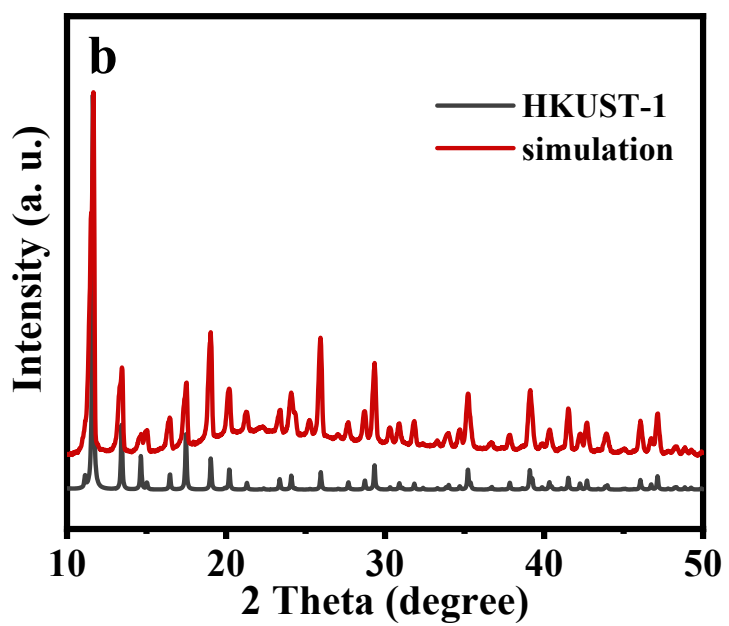
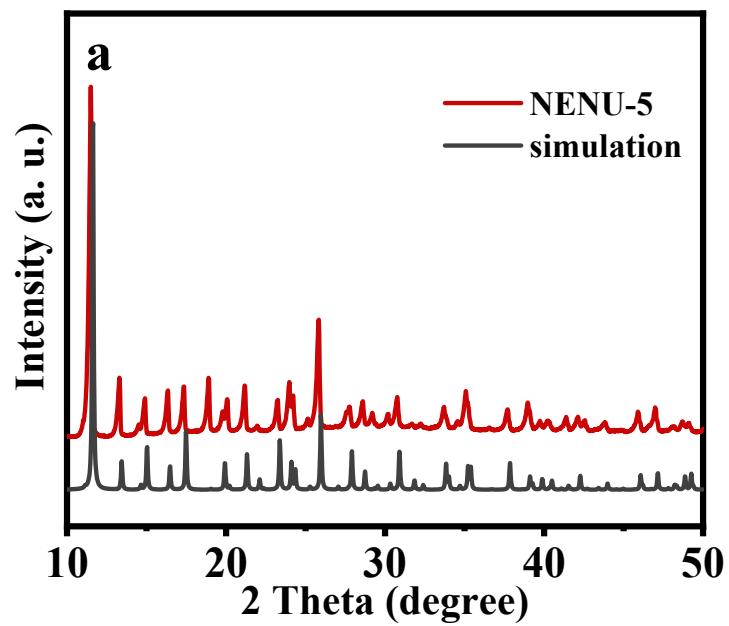


Fig. S2 XRD pattern of (a) NENU-5 and (b) HKUST-1.

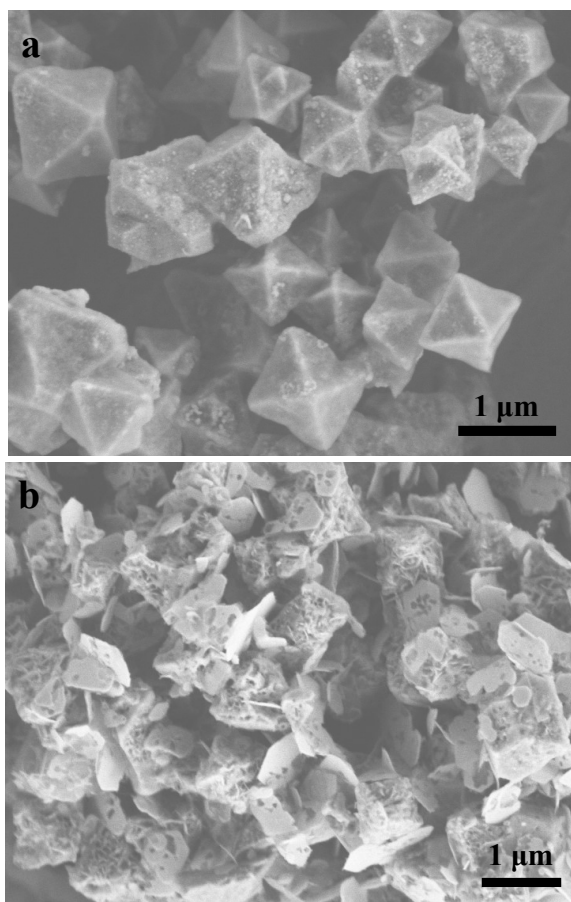


Fig. S3 SEM images of (a) C-MoO₂ and (b) C-MoO₂/MoS₂.

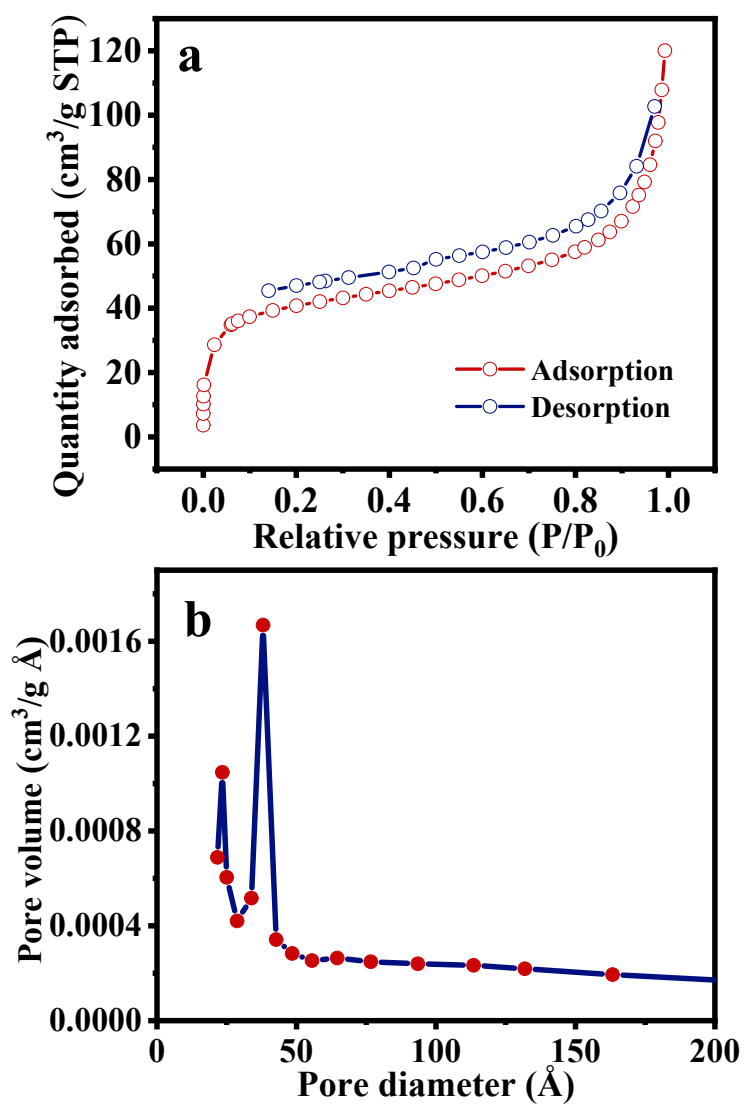


Fig. S4 (a) N₂ adsorption-desorption isotherm of C-MoO₂/MoS₂, (b) pore size distribution curve of C-MoO₂/MoS₂.

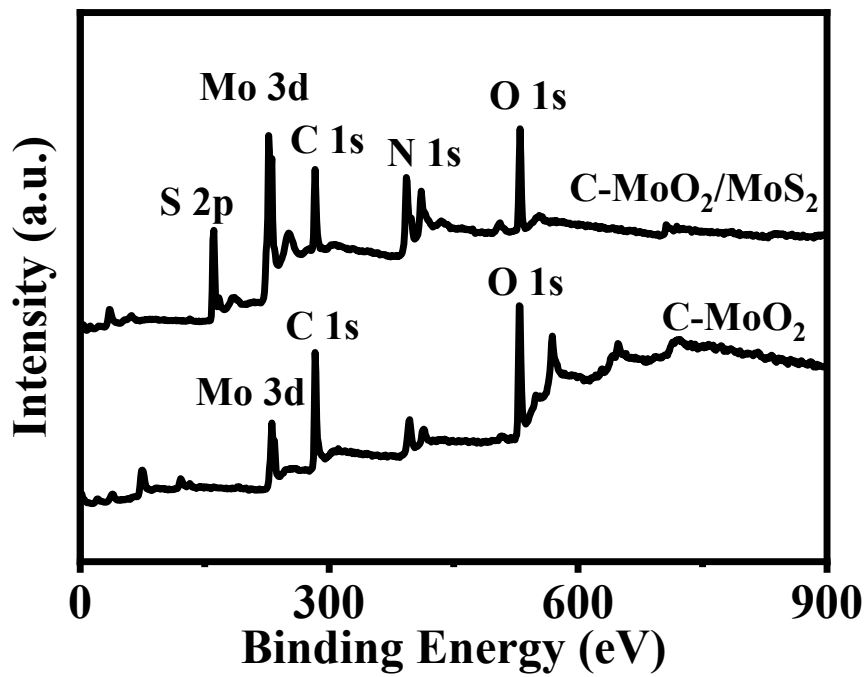


Fig. S5 The survey XPS spectra of C-MoO₂ and C-MoO₂/MoS₂.

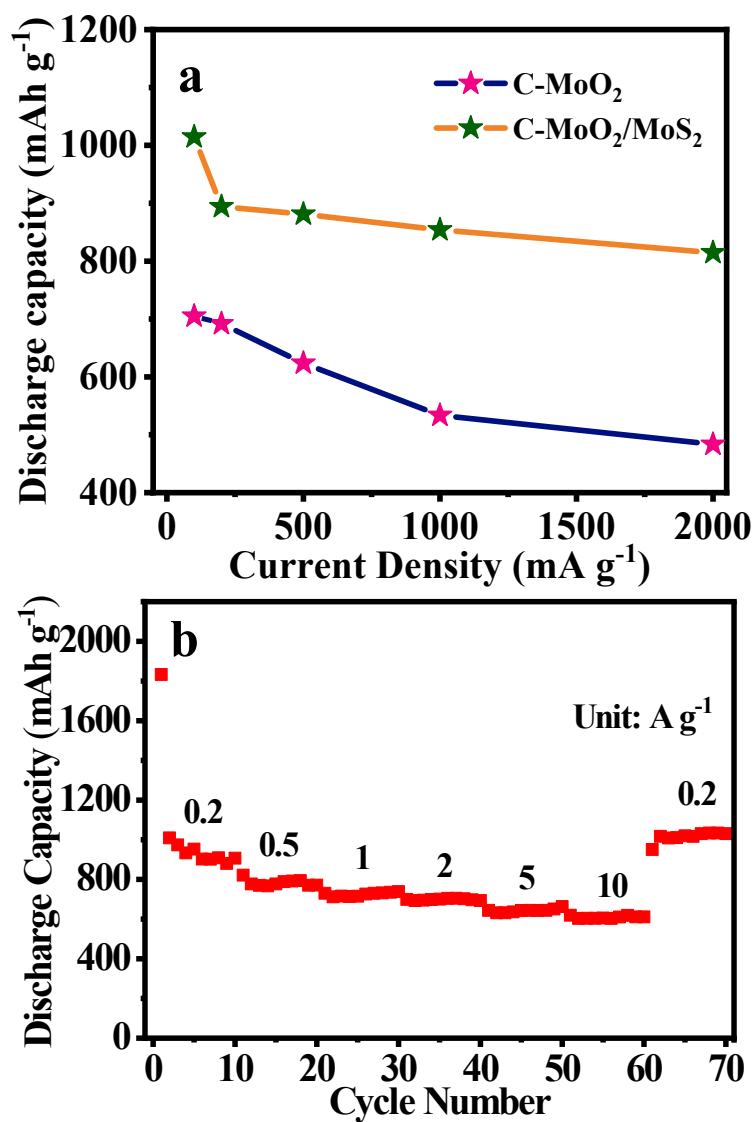


Fig. S6 (a) The capacity retention of C-MoO₂ and C-MoO₂/MoS₂ at 100, 200, 500, 1000, and 2000 mA g⁻¹, (b) rate capability of C-MoO₂/MoS₂ at 0.2, 0.5, 1, 2, 5, and 10 A g⁻¹.

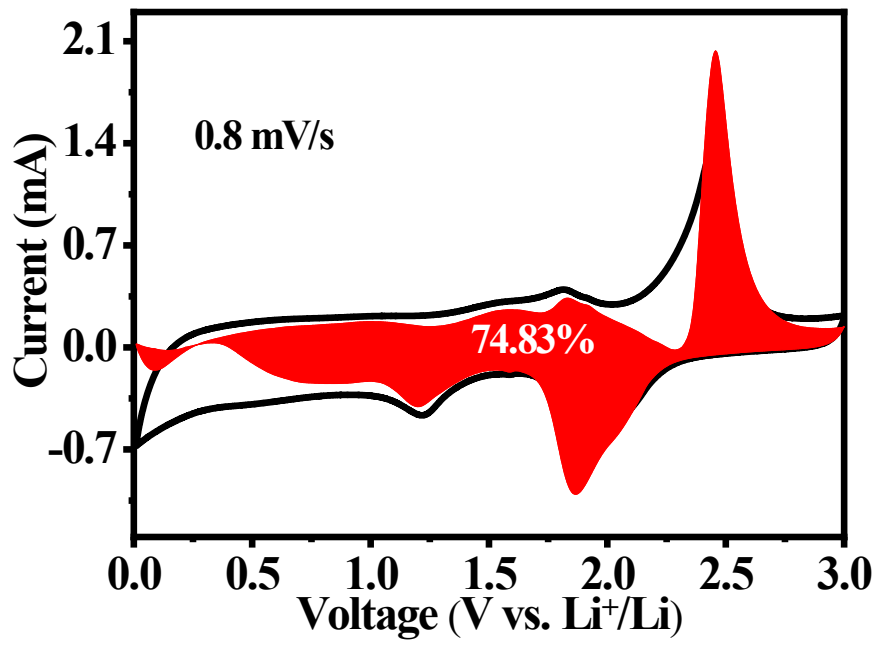


Fig. S7 Capacitive contribution (shaded region) of C-MoO₂/MoS₂ at the scan rate of 0.8 mV s⁻¹.

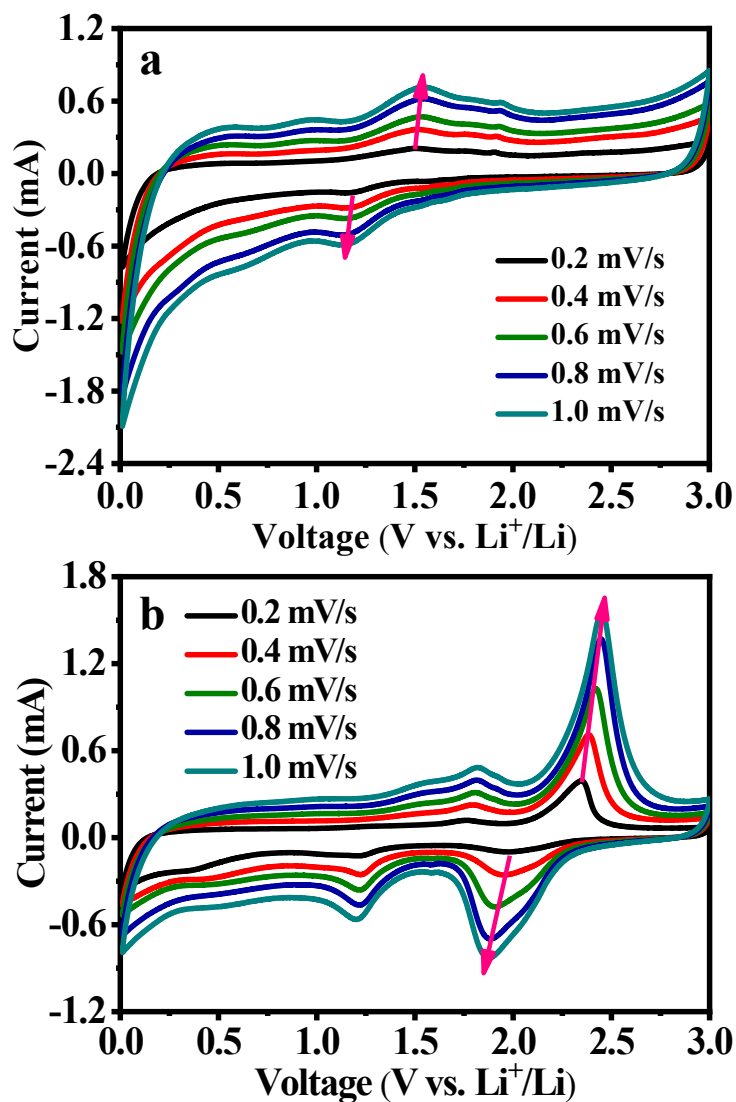


Fig. S8 CV curves of (a) C-MoO₂ and (b) C-MoO₂/MoS₂ in the potential range of 0.01~3.0 V with different scan rates (0.2, 0.4, 0.6, 0.8 and 1.0 mV s⁻¹). CV data is collected once the cell is post run for the first cycle to allow the formation of the SEI layer.

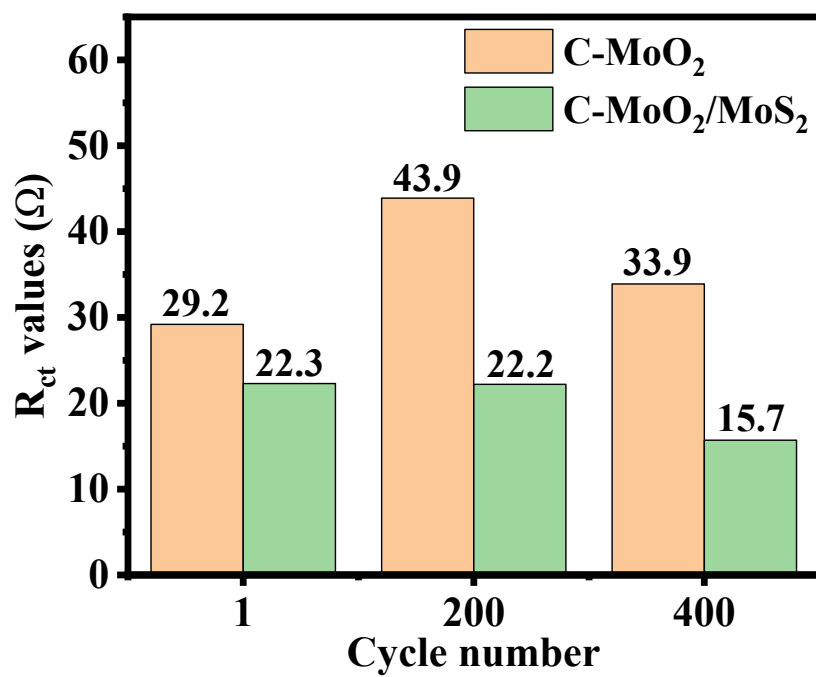


Fig. S9 The R_{ct} values of the C-MoO₂ and C-MoO₂/MoS₂.

Table S1 Rate performance of C-MoO₂/MoS₂ compared with other previously reported MoO₂/MoS₂-based anodes in the literatures.

Sample	Synthetic method	Potential range	Rate capabilities	Reference
MoO ₂ /MoS ₂ /C	Carbonization	0.01-3.0 V	486 mAh g ⁻¹ at 5 A g ⁻¹	[1]
MoO ₂ @MoS ₂ -91	Annealing MoO ₂ with S powder under Ar	0.01-3.0 V	430 mAh g ⁻¹ at 5 A g ⁻¹	[2]
POM-CS	Annealing POM-900 with S powder under vacuum	0.1-3.0 V	380 mAh g ⁻¹ at 5 A g ⁻¹	[3]
MoO ₂ @MoS ₂	Roasting Mo powder with gas flow of N ₂ -SO ₂	0.01-3.0 V	578 mAh g ⁻¹ at 5 A g ⁻¹	[4]
cw-MoO ₂ @MoS ₂	Calcining MoO ₃ under H ₂ S	0.01-3.0 V	344 mAh g ⁻¹ at 10 A g ⁻¹	[5]
MoO ₂ /MoS ₂	Hydrothermal reaction	0.01-3.0 V	273 mAh g ⁻¹ at 6.4 A g ⁻¹	[6]
MO/MS/SG-1	Hydrothermal reaction and sulfuration	0-3.0 V	222 mAh g ⁻¹ at 3 A g ⁻¹	[7]
MoO ₂ @MoS ₂ /rGO	Sulfuration and hydrothermal reaction	0.01-3.0 V	645 mAh g ⁻¹ at 4 A g ⁻¹	[8]
MoO ₂ @MoS ₂	Hydrothermal reaction	0.01-3.0 V	700 mAh g ⁻¹ at 1 A g ⁻¹	[9]
MoO ₂ -QDs@RGO	Hydrothermal reaction	0-3.0 V	619 mAh g ⁻¹ at 2 A g ⁻¹	[10]
C-MoO ₂ /MoS ₂	Annealing C-MoO ₂ with S powder under N ₂	0.01-3.0 V	610 mAh g ⁻¹ at 10 A g ⁻¹	This work

References

1. X. F. Liu, P. Mei, Y. Dou, R. Luo, Y. Yamauchi and Y. K. Yang, *J. Mater. Chem. A*, 2021, **9**, 13001-13007.
2. Z. Xu, T. Wang, L. Kong, K. Yao, H. Fu, K. Li, L. Y. Cao, J. F. Huang, and Q. L. Zhang, *Part. Part. Syst. Charact.*, 2017, **34**, 1600223.
3. C. L. Wu, J. L. Hu, Z. G. Yao, D. G. Yin and C. L. Li, *ACS Appl. Mater. Interfaces*, 2019, **11**, 23280-23290.

4. H. Sun, J. L. Xu, J. D. Huang, G. H. Li, J. Luo, M. J. Rao, Z. W. Peng and T. Jiang, *J. Alloys Compd.*, 2021, **851**, 156726.
5. D. B. Xiao, J. Y. Zhang, X. Li, D. Zhao, H. Y. Huang, J. L. Huang, D. X. Cao, Z. H. Li and C. M. Niu, *ACS Nano*, 2016, **10**, 9509-9515.
6. Z. N. Deng, Y. J. Hu, D. Y. Ren, S. L. Lin, H. Jiang and C. Z. Li, *Chem. Commun.*, 2015, **51**, 13838-13841.
7. Y. Q. Zhang, H. C. Tao, H. Ma, S. L. Du, T. Li, Y. K. Zhang, J. H. Li and X. L. Yang, *Electrochim. Acta*, 2018, **283**, 619-627.
8. R. Zhang, Z. Tang, H. Y. Wang, D. Sun, Y. G. Tang and Z. Y. Xie, *Electrochim. Acta*, 2020, **364**, 136996.
9. J. R. Xie, K. J. Zhu, J. Min, L. Y. Yang, J. Z. Luo, J. Liu, M. Lei, R. Z. Zhang, L. Ren and Z. Y. Wang, *Ionics*, 2019, **25**, 1487-1494.
10. C. D. Wang, J. J. Jiang, Y. J. Ruan, X. Ao, K. Ostrikov, W. J. Zhang, J. Lu and Y. Y. Li, *ACS Appl. Mater. Interfaces*, 2017, **9**, 28441–28450.